Mechanism of O_2 Activation by Cytochrome P450cam Studied by Isotope Effects and Transient State Kinetics†

Matthew M. Purdy,‡,§ Laura S. Koo,|| Paul R. Ortiz de Montellano,|| and Judith P. Klinman*,‡,⊥

Department of Chemistry and Department of Molecular and Cell Biology, University of California, Berkeley, California 94720-1460, and Department of Pharmaceutical Chemistry, University of California, San Francisco, California 94143-2280

Received August 22, 2006; Revised Manuscript Received October 9, 2006

ABSTRACT: The early steps in dioxygen activation by the monooxygenase cytochrome P450cam (CYP101) include binding of O_2 to ferrous P450cam to yield the ferric-superoxo form (oxyP450cam) followed by an irreversible, long-range electron transfer from putidaredoxin to reduce the oxyP450cam. The steady state kinetic parameter $k_{cat}/K_m(O_2)$ has been studied by a variety of probes that indicate a small D_2O solvent isotope effect (1.21 ± 0.08), a very small solvent viscosogen effect, and a $^{16}O/^{18}O$ isotope effect of 1.0147 ± 0.0007. This latter value, which can be compared with the $^{16}O/^{18}O$ equilibrium isotope effect of 1.0048 ± 0.0003 measured for oxyP450cam formation, is attributed to a primarily rate-limiting outer-sphere electron transfer from the heme iron center as O_2 that has prebound to protein approaches the active site cofactor. The electron transfer from putidaredoxin to oxyP450cam was investigated by rapid mixing at 25 °C to complement previous lower-temperature measurements. A rate of 390 ± 23 s^{-1} (and a near-unity solvent isotope effect) supports the view that the long-range electron transfer from reduced putidaredoxin to oxyP450cam is rapid relative to dissociation of O_2 from the enzyme. P450cam represents the first enzymatic reaction of O_2 in which both equilibrium and kinetic $^{16}O/^{18}O$ isotope effects have been measured.

The bacterial monooxygenase cytochrome P450cam[1] (CYP101) has a well-studied mechanism for molecular oxygen activation and camphor hydroxylation (*1*, *2*). Turnover by the heme-containing P450cam is supported by a pair of electron-carrying proteins, the iron−sulfur cluster-containing putidaredoxin (Pdx) and the flavoprotein putidaredoxin reductase (PdR). Most evidence (*2*−*4*), including our own recent work (*5*), points toward an electron transport mechanism in which Pdx acts as a diffusible shuttle for the transfer of electrons from PdR to P450cam. The overall turnover rate of P450cam requires two long-range electron transfer steps from the reduced form of putidaredoxin (Pdx^r) to P450cam (*2*, *3*). The first of these electron transfer steps (governed by $k_{et,1}$ in Scheme 1) produces the ferrous, camphor-bound form of P450cam (Fe^{2+}cam) and is proposed to limit turnover when Pdx^r and all substrates are saturating (k_{cat} conditions) (*3*).

The work presented here addresses the early steps in O_2 activation by examining the steady state kinetic parameter $k_{cat}/K_m(O_2)$, which includes the steps from O_2 binding up to the first kinetically irreversible step. As highlighted in Scheme 1 for the case of P450cam, these potentially include the reaction of O_2 with Fe^{2+}cam to yield the well-characterized (*1*, *6*−*8*) oxygenated myoglobin-like ferric-superoxo intermediate (oxyP450cam) and the long-range electron transfer step from Pdx^r to oxyP450cam to produce a ferric-peroxo intermediate (governed by $k_{et,2}$ in Scheme 1). The ferric-peroxide intermediate has been observed following radiolytic reduction at cryogenic temperatures (*1*, *9*), but Brewer and Peterson (*3*, *10*) demonstrated that oxyP450cam is the last observable intermediate in the solution phase reaction with Pdx^r as the electron donor. They showed that the oxidation of Pdx^r, disappearance of oxyP450cam, and appearance of product all occur at the same rate, indicating that this long-range electron transfer step is kinetically irreversible. In a more recent investigation of this reaction, Glascock et al. (*11*) demonstrated the buildup of a spectrally perturbed form of oxyP450cam but did not detect any ferric-peroxo or ferryl-oxo species during the reaction between

† This work was supported by National Institutes of Health Grants GM 25765 (to J.P.K.) and GM 25515 (to P.R.O.d.M.). M.M.P. was supported in part by National Institutes of Health Biophysics Pre-Doctoral Training Grant 5 T32 GM 08295-13.

* To whom correspondence should be addressed. Phone: (510) 642-2668. Fax: (510) 643-6232. E-mail: klinman@berkeley.edu.

‡ Department of Chemistry, University of California, Berkeley.

§ Present address: Department of Chemistry and Biochemistry, University of California, Santa Barbara, CA 93106-9510.

|| University of California, San Francisco.

⊥ Department of Molecular and Cell Biology, University of California, Berkeley.

[1] Abbreviations: P450cam, cytochrome P450cam (CYP101) from *Pseudomonas putida*; Fe^{2+}cam, camphor-bound ferrous P450cam; Fe^{3+}-cam, camphor-bound ferric P450cam; oxyP450cam, camphor- and oxygen-bound P450cam; Fe^{3+}mtp, metyrapone-bound ferric P450cam; Fe^{2+}mtp, metyrapone-bound ferrous P450cam; Fe^{2+}cam-CO, camphor- and carbon monoxide-bound ferrous P450cam; PdR, putidaredoxin reductase; Pdx, putidaredoxin; Pdx^r, reduced form of putidaredoxin; KIE, kinetic isotope effect; EIE, equilibrium isotope effect; ^{18}k (or ^{18}K), $^{16}O/^{18}O$ isotope effect on a rate (or equilibrium) constant, i.e., rate (or equilibrium) constant with $^{16}O^{16}O$ dioxygen divided by that with $^{16}O^{18}O$ dioxygen; $^{D_2O}(k)$, solvent isotope effect on a kinetic parameter, i.e., parameter in H_2O divided by that in D_2O; MOPS, 3-(*N*-morpholino)-propanesulfonic acid; DTT, dithiothreitol; PCD, protocatechuate 3,4-dioxygenase; PCA, protocatechuic acid.

10.1021/bi061726w CCC: $33.50
Published on Web 12/05/2006

Scheme 1: Catalytic Cycle of P450cam with Steps Potentially Involved in $k_{cat}/K_m(O_2)$ Highlighted in the Dashed Box[a]

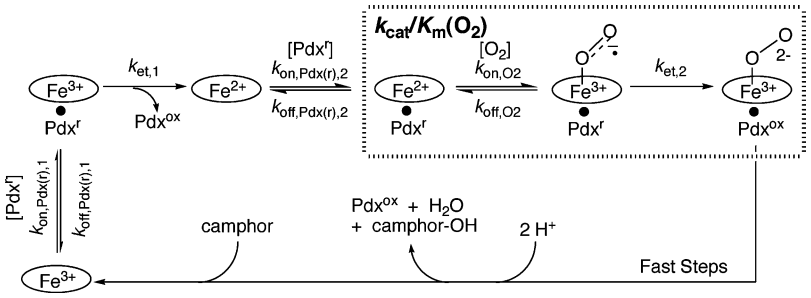

[a] Camphor is bound to all P450cam forms that are drawn.

oxyP450cam and Pdx^r. The authors suggested that altered hydrogen bonding at the heme thiolate ligand is the cause of the spectral perturbation. Such changes have been proposed to tune the reduction potential of oxyP450cam allowing reduction by Pdx^r and to facilitate O−O bond cleavage (*11*−*14*).

Previously, we suggested that $k_{et,2}$ contributes partially to $k_{cat}/K_m(O_2)$, in P450cam on the basis of a comparison of $k_{cat}/K_m(O_2)$ to k_{on,O_2} (*5*). Some recent evidence indirectly suggests that complexation of Pdx^r to P450cam can influence binding of ligands at the heme iron (*12*−*16*). The measurements presented in this work, the impact of solvent viscosogens on $k_{cat}/K_m(O_2)$, together with D_2O solvent and $^{16}O/^{18}O$ kinetic isotope effects (KIEs), provide further insight into the rate-limiting steps contributing to the interaction of O_2 with enzyme (cf. Scheme 1). We have also used stopped-flow methods to examine the nature of the second long-range electron transfer step from Pdx^r to oxyP450cam at 25 °C, expanding on previous measurements at lower temperatures (*3*, *17*). The aggregate results indicate that $k_{cat}/K_m(O_2)$ is primarily limited by the addition of O_2 to the heme iron, with the subsequent electron transfer from Pdx^r occurring relatively rapidly ($k_{off,O_2} < k_{et2}$).

In previous studies, a significant D_2O effect had been reported for the reduction of oxyP450cam by putidaredoxin at 8 °C (*17*), suggesting the importance of proton coupling during this long-range electron transfer. The significance of proton transfer during this step was later heightened upon finding a very large solvent isotope effect on the D251N mutant where the rate of Pdx^r to oxyP450cam electron transfer is slowed greatly (*18*, *19*). Our measurements, which indicate a solvent isotope effect on the second electron transfer step that is close to unity, suggest that proton coupling may not be contributing to the long-range electron transfer for the wild-type enzyme at 25 °C.

In recent years, a number of studies have addressed the early steps in O_2 activation for a range of enzymes, with a common theme emerging in which the introduction of the first electron into O_2 (reducing the formal bond order from 2 to 1.5) is a major rate-limiting step (*20*). These studies include reactions between O_2 and organic cofactors in glucose oxidase (*21*−*23*), amine oxidase (*24*−*26*), and tyrosine hydroxylase (*27*) or with a binuclear iron center in methane monooxygenase (*28*). In each of these cases, the $^{16}O/^{18}O$ kinetic isotope effect (KIE) on $k_{cat}/K_m(O_2)$ was an important factor in determining the nature of the first committed step in O_2 activation. In this study, it has also been possible to measure the $^{16}O/^{18}O$ equilibrium isotope effect (EIE) when O_2 binds to the enzyme, showing an effect similar to that in earlier studies with myoglobin (*29*). The ability to examine kinetic and equilibrium $^{16}O/^{18}O$ isotope effects in a single enzyme system further enables the mechanistic interpretation in O_2-activating enzymes.

EXPERIMENTAL PROCEDURES

Materials. MOPS, DTT, NADH, (1*R*)-(+)-camphor, D_2O (99.9 at. % D), KOD (98 at. % D), metyrapone (2-methyl-1,2-dipyridyl-1-propanone), pyrogallol (1,2,3-trihydroxybenzene), glucose oxidase (lyophilized powder, type X-S, from *Aspergillus niger*), β-D-(+)-glucose for the O_2 scrubbing system, protocatechuic acid (3,4-dihydroxybenzoic acid) and protocatechuate 3,4-dioxygenase (from *Pseudomonas* sp.), sodium dithionite (sodium hydrosulfite, technical grade, ~85%), and myoglobin (from horse skeletal muscle) were products of Sigma-Aldrich. Sucrose, glycerol, and glucose for viscosity effect studies were ACS reagent-grade. Catalase (from beef liver, suspension in water) was a product of Roche. Biogel P6-DG resin was purchased from Bio-Rad. The protocatechuic acid was recrystallized from water, using activated carbon to decolorize the heated solution. Camphor was delivered to buffers from a 1 or 2 M stock solution in ethanol. Pdx, PdR, wild-type P450cam, and N-terminally $(His)_6$-tagged P450cam were obtained and quantitated as described previously (*5*). The $(His)_6$-tagged P450cam was used in all experiments, except as noted. Unless otherwise noted, all reactions were carried out in a buffer of 50 mM MOPS and 69 mM KCl titrated to pH 7.4 with KOH, termed "standard buffer".

The preparation of the $(His)_6$P450cam used in the stopped-flow and equilibrium isotope effect experiments was somewhat different from the literature procedure (*30*). After the nickel−NTA−agarose column, a phenyl-Sepharose hydrophobic interaction column was employed to remove a lower-molecular weight contaminating protein, presumably a $(His)_6$-tagged proteolytic fragment. Despite the extra purification step, this preparation was less pure, with an A_{391}/A_{280} ratio of 1.2 (compared to 1.5 for the more pure $(His)_6$P450cam preparation used in steady state experiments). This less pure preparation gave the same results as the wild type in the O_2 binding stopped-flow measurements. The two different $(His)_6$ preparations gave the same results in preliminary stopped-flow reactions between Pdx^r and oxyP450cam. The less pure $(His)_6$P450cam was not used in steady state measurements, but rather only in experiments where the results were expected to be independent of enzyme concentration (O_2 binding and single turnover).

Stable isotope ratio mass spectrometry on CO_2 samples was performed at either Geochron Laboratories in Cam-

bridge, MA, or the Colorado Plateau Stable Isotope Laboratory at Northern Arizona University in Flagstaff, AZ.

Effects of Viscosity on Steady State Parameters. Initial rates were determined by O_2 consumption as described previously (*5*). Rates were determined at 25 °C in the standard buffer containing 500 μM camphor, 500 μM NADH, and 100 μM DTT. The amount of PdR required for saturation was re-determined at the highest concentration of each of the three viscosogens employed, and limiting kinetic parameters at saturating PdR were determined by varying the O_2 and Pdx concentrations followed by fitting to the equation for a sequential ordered mechanism as described previously (*5*).

Viscosities were modulated by inclusion of 23.4% glucose, 31.4% glycerol, 27.4% glucose, 35.2% glycerol, or 37.2% sucrose in the buffer solutions (expressed in weight to weight percent). They gave viscosities relative to aqueous buffer with no added viscosogen of 2.20, 2.38, 2.63, 2.98, and 5.00 at 25 °C. Relative viscosities were determined as previously described (*31*). The decreases in apparent O_2 solubility in the solutions of various viscosogens were determined by an end-point assay using protocatechuate 3,4-dioxygenase (PCD) with limiting protocatechuic acid (PCA), a substrate known to be consumed in a 1:1 stoichiometry with O_2 (*32*). The correction factors obtained in this assay are a combination of O_2 solubility and electrode response.

Solvent Isotope Effects on Steady State Parameters. Initial rates were measured as described above. The standard buffer was prepared in D_2O by dissolving MOPS and KCl in D_2O and then titrating to pD 7.4 with a KOD solution. A value of 0.4 was added to the reading on the pH meter to correct to pD (*33*). The buffer was lyophilized and redissolved in D_2O twice. After the pD had been readjusted, camphor was added. In parallel, a buffer was prepared in H_2O for direct comparison. Protein solutions were prepared in both D_2O and H_2O. $(His)_6$P450cam in D_2O was prepared as described in ref *5* but using the D_2O buffer in the G-25 column during DTT removal. Pdx and PdR were exchanged into the D_2O buffer using Amicon microcentrifuge concentrators. To avoid H_2O contamination in the D_2O reactions, the electrode tip was soaked in D_2O before being blotted dry prior to each reaction and D_2O was placed in the bubbler which humidified the mixture of O_2 and N_2 gases used to vary the O_2 concentration.

General Transient State Kinetic Methodology. Measurements were carried out on a Hi-Tech SF-61 DX2 stopped-flow system using a xenon lamp and photodiode array detection with a 1.5 ms signal integration time. The observation cell had an optical path length of 1.0 cm. Solutions containing P450cam or Pdx were deoxygenated over a period of ~45 min by seven to nine cycles of evacuation under house vacuum followed by equilibration with argon. The argon was scrubbed of residual O_2 by being passed through one bubbling tower of a solution containing pyrogallol and NaOH. Protein solutions were kept on ice during deoxygenation and then allowed to warm to room temperature while being reduced by NADH with catalytic amounts of PdR (and Pdx in the case of P450cam reductions) for 15−25 min before samples were loaded into the drive syringes. The drive syringes and flow circuitry were flushed with argon-saturated water prior to the loading of the protein samples. Samples were allowed to stand in the drive syringes for approximately 5 min before data for the first reaction were acquired. Despite all efforts, the anaerobicity of the solutions was incomplete unless an O_2 scrubbing system was employed (see below).

A dead time of 1.1 ± 0.1 ms was measured using the reaction of 2,6-dichlorophenolindophenol with ascorbic acid (*34*). The middle of the 1.5 ms signal integration time is taken to be the time point for each spectrum. The first spectrum then occurs at 1.9 ms (1.1 ms + 1.5 ms/2) after mixing. The reaction rates were linear with ascorbic acid concentration up to at least 600 s^{-1} despite a long signal integration time.

Reaction between O_2 and Ferrous P450cam. Solutions of P450cam were reduced anaerobically and then mixed with an equal volume of an O_2-containing solution using the stopped-flow instrument. The measurements were performed at 25 °C by methods similar to those previously employed at 4 °C (*8*). Camphor was present at a concentration of 500 μM in all buffers used in this experiment. The O_2-containing solutions employed were either a buffer saturated with air at 25 °C (to give 129 μM O_2 after mixing) or a combination of air- and argon-saturated buffers mixed using two syringes connected by a short piece of tubing after all gas head space had been eliminated. The solutions of 4 or 8 μM P450cam were reduced using 50−100 μM NADH and small amounts of Pdx (0.04−0.2 μM) and PdR (0.1−0.4 μM), where the noted concentrations are before stopped-flow mixing. The final concentration of P450cam was kept at least 10-fold lower than that of O_2 to maintain pseudo-first-order conditions. Both $(His)_6$-tagged and wild-type P450cam were used in these measurements. The observed rates were identical and hence combined to give the data presented in the Results.

Reaction between Pdx^r and OxyP450cam. The stopped-flow instrument was used in double-mixing mode. Anaerobically reduced P450cam (solution A) was rapidly mixed with an equal volume of O_2-saturated buffer (solution B) to form oxyP450cam. After a delay time of 20−100 ms, the newly formed oxyP450cam solution was rapidly mixed against an equal volume of Pdx^r (solution C) to start the reaction. Following the reaction between Pdx^r and oxyP450cam, the resting form of the enzyme is trapped by a large concentration of the inhibitor metyrapone as in the method developed by Brewer and Peterson (*3*, *10*).

An O_2 scrubbing system consisting of glucose, glucose oxidase, and catalase at concentrations similar to those employed in previous studies (*3*, *4*, *10*) was included with the P450cam and Pdx^r solutions. As described below, oxyP450cam is the observed product of the first mixing step. This indicates that the level of O_2 scrubbing employed here is sufficient to remove O_2 which leaks into the sample during preparation but not so high as to consume all of the intentionally added O_2 (from solution B) during the delay time between the first and second stages of mixing. All solutions were made in the standard buffer. Solution A consisted of 20 μM P450cam, 100 μM camphor (including that bound to the enzyme), 120 mM glucose, 3000 units/mL catalase, and catalytic concentrations of Pdx and PdR (0.1 μM each). After deoxygenation, glucose oxidase (0.2 mg/mL) and NADH (100 μM) were added to solution A. Solution B consisted of standard buffer saturated with O_2 at room temperature by bubbling (~1.2 mM at 1 atm of O_2 and 25 °C). Solution C contained 50 μM Pdx, 5.0 mM metyrapone, 120 mM glucose, 1500 units/mL catalase, and

a catalytic concentration of PdR (0.05 μM). After deoxygenation, glucose oxidase (0.05 mg/mL) and NADH (250 μM) were added to solution C. The concentrations in the reaction after the final stage of mixing were 5.0 μM P450cam, 25 μM total camphor, ~300 μM O_2, 25 μM Pdx, and 2.5 mM metyrapone.

UV−visible spectra for comparison to the stopped-flow data (Figure 2C) were recorded on a Cary 3B spectrophotometer using methods similar to those from ref *8*. Briefly, ferrous samples were prepared by dithionite reduction. OxyP450cam was prepared by addition of an equal volume of O_2-saturated buffer to the Fe^{2+}cam form at 4 °C followed by correction for the dilution. Fe^{3+}cam, Fe^{3+}met, and Fe^{2+}-met were prepared at room temperature.

To measure the solvent isotope effect on this reaction, the standard buffer was prepared in D_2O as described for the steady state measurements, except the buffer was not lyophilized from D_2O for the stopped-flow measurements. Solutions A−C were made up in the D_2O-containing buffer, and the protein stock solutions were exchanged into this buffer by the methods described above. The final reaction mixture was approximately 99.4 at. % D. It was necessary to incubate the D_2O-containing buffers at room temperature for ~45 min after addition of the catalase to dissolve the suspension. To minimize H_2O contamination, the drive syringes and flow circuitry were flushed with argon-saturated D_2O prior to loading the reactants. Additionally, a bubbling tower of D_2O was placed on the argon supply line following the bubbling tower containing the pyrogallol/NaOH solution in H_2O.

Equilibrium Isotope Effect on O_2 Binding. All manipulations were carried out in 50 mM potassium phosphate buffer (pH 7.4) containing 1 mM camphor. A 700−1000 μM P450cam solution was incubated with 10 mM DTT for 30 min at 25 °C to eliminate disulfide-induced dimerization and then flushed with argon. The remaining sample preparation procedures were carried out at 4−6 °C. P450cam was reduced using excess sodium dithionite with spectrophotometric monitoring to confirm complete conversion to the Fe^{2+}cam form. P450cam was separated from dithionite and DTT using a Biogel P6-DG desalting column. The colored elutant was stirred rapidly for 7−8 min under air to re-equilibrate the sample with atmospheric O_2, forming oxyP450cam. The sample was diluted to ~20 mL with buffer pre-equilibrated with air in an open sample chamber which was thermostated at 4 °C and connected to the vacuum line. After a total of 10−12 min had elapsed since the removal of sodium dithionite, an 11 mL portion of the oxyP450cam sample was introduced into the vacuum line.

The total O_2 in this sample (the sum of that bound to P450cam and that dissolved in solution) was isolated and converted to CO_2, and the isotope effect on the equilibrium constant for O_2 binding was calculated from the observed pressure of the CO_2 and its ^{16}O:^{18}O isotope ratio as described previously (*29*) with modifications detailed in ref *35*. The main modifications were designed to minimize the loss of P450cam-bound O_2 as $O_2^{\bullet-}$ by the autoxidation reaction (*8*) in the ~1 h required to collect the O_2 from the sample. Potassium ferricyanide, which reacts with oxyP450cam to give O_2 and Fe^{3+}cam within several seconds at the concentrations employed here, was included inside the vacuum line. This reaction preserves all of the oxygen bound to P450cam at the time of introduction into the vacuum line as O_2, preventing release of $O_2^{\bullet-}$ during the ~1 h required to collect the O_2 gas from the sample.

The extent of autoxidation of oxyP450cam during sample handling prior to introduction into the vacuum line was determined by following the continuing exponential decay of the excess oxyP450cam solution remaining in the sample chamber. Spectrophotometric monitoring at 4 °C for several hours allowed extrapolation to infinite time to give the total concentration of P450cam. Extrapolation back in time to the point where the sample was taken into the vacuum line gave the fraction of P450cam remaining in the O_2-bound form.

Following each experiment, the P450cam sample was recovered from the vacuum line and sample chamber and then dialyzed to remove potassium ferricyanide. The sample was concentrated, centrifuged to remove precipitated protein, and reused. The $^{18}K_{O_2}$ reported in the Results is the average of three measurements taken from the same P450cam sample used three times. The small error and the lack of a trend in the measured EIE (Figure 3A) indicates that protein damage capable of affecting O_2 binding was minimal.

Kinetic Isotope Effect on O_2 Consumption. The KIE on oxygen consumption by the P450cam system was determined at 25 °C in standard buffer containing 1 mM camphor by minor modifications to published procedures (*36*). A mixture of O_2-saturated and vacuum-degassed buffers was made to yield a final concentration of ~440 μM O_2. The O_2 concentration was lowered from the value of ~1.2 mM employed previously to minimize the contribution of the background O_2 consumption by NADH, Pdx, and PdR. This solution was sealed into a reaction chamber connected to a vacuum line. After O_2 had been collected from a blank sample, P450cam, Pdx, and PdR were injected into the ~26 mL of remaining solution. To start the reaction, NADH (0.5−1.0 mM final concentration) was injected along with DTT (0.1 mM final concentration). The reaction was allowed to proceed for 3−15 min to give 30−70% consumption of the O_2. A 16 mL sample of the reaction mixture was then taken into the vacuum line and the reaction quenched, and the O_2 was collected and converted to CO_2 as previously reported (*36*). Calculation of the $^{16}O/^{18}O$ isotope effect on O_2 consumption, $^{18}k_{obs}$, from the measured CO_2 pressures and isotope ratios of the blank and reaction time point samples was carried out as described previously (*24*).

Both the rates of the background reaction in the absence of P450cam in relation to the rate of P450cam-catalyzed O_2 consumption and the PdR concentration required to saturate the system at the given concentrations of Pdx and P450cam were determined under conditions employed in the KIE measurements using previously described (*5*) initial rate assays.

RESULTS

Solvent Isotope Effects on Steady State Parameters. The solvent kinetic isotope effects on the apparent $k_{cat}/K_m(O_2)$ and k_{cat} were measured at 8 μM Pdx with a saturating PdR concentration. Under these conditions, the apparent k_{cat}/K_m-(O_2) is independent of the Pdx^r concentration and the apparent k_{cat} is near saturation (*5*). The kinetic parameters were similar, whether the three proteins were added to the assay mixture from either D_2O or H_2O stock solutions,

Table 1: Solvent Isotope Effects on Apparent Steady State Parameters[a]

[Pdx] (mM)	$^{D_2O}[k_{cat}/K_m(O_2)]$	$^{D_2O}(k_{cat})$[e]	% D[f]
8.0[b]	1.3 (1)	0.97 (4)	99.2
8.0[c]	1.21 (8)	0.97 (4)	99.9
15.0[d]	1.14 (8)	1.02 (3)	99.8

[a] Conditions as described in the legend of Figure 1 except pH/pD 7.4, and kinetic parameters are not extrapolated to an infinite Pdx^r concentration and are therefore apparent steady state parameters. Errors in the last digit are in parentheses. [b] Pdx, PdR, and P450 delivered from H_2O stock solutions. [c] Pdx, PdR, and P450 delivered from D_2O stock solutions. [d] P450 delivered from a H_2O stock solution in all reactions. Pdx and PdR delivered from H_2O solutions for reactions in H_2O but from D_2O stock solutions for reactions in D_2O. [e] The observed $^{D_2O}(k_{cat})$ values were multiplied by 0.933 to normalize for a 7% increase in the apparent O_2 solubility/electrode response in the D_2O-containing buffer over that in H_2O as determined by the PCA/PCD O_2 electrode calibration assay. [f] Final atom % D in the D_2O buffer.

Table 2: Effect of pH on Kinetic Parameters[a]

pH	[Pdx^r] (μM)	apparent $k_{cat}/K_m(O_2)$ (μM^{-1} s^{-1})	apparent k_{cat} (s^{-1})
6.9	8.0	0.68 ± 0.04	46 ± 1
6.9	**15.0**	$\mathbf{0.70 \pm 0.05}$	$\mathbf{47 \pm 2}$
7.4	8.0	0.65 ± 0.05	44 ± 2
7.4	**15.0**	$\mathbf{0.67 \pm 0.03}$	$\mathbf{51 \pm 2}$
7.9	8.0	0.52 ± 0.01	33 ± 1
7.9	**15.0**	$\mathbf{0.51 \pm 0.03}$	$\mathbf{39 \pm 1}$

[a] Apparent kinetic parameters from O_2 variation at 8 and 15 μM Pdx^r. Conditions: 50 mM MOPS-KOH buffer at the noted pH with sufficient KCl to give an ionic strength of 0.1 M, 100 μM DTT, and 13 nM P450cam, with saturating PdR, NADH, and camphor concentrations. Values at 15 μM Pdx^r are closer approximations to the limiting kinetic parameters at Pdx^r saturation and hence highlighted in bold.

indicating that a change in protein structure due to replacement of slowly exchanging backbone amide protons with deuterons does not influence the measured solvent isotope effects. To verify that D_2O does not grossly perturb the amount of Pdx^r required for saturation, O_2 variation was repeated at 15 μM Pdx^r with insignificant changes in the D_2O effects. The values for the solvent isotope effects on the apparent kinetic parameters for the two experiments at 8 μM Pdx^r and one at 15 μM Pdx^r are listed individually in Table 1 and are averaged here to give a D_2O effect of 1.21 $\pm$ 0.08 on $k_{cat}/K_m(O_2)$ and 0.99 $\pm$ 0.02 on k_{cat}.

As shown in Table 2, the apparent k_{cat} and $k_{cat}/K_m(O_2)$ are not very pH-dependent over the narrow range of 6.9−7.9, which brackets the pH used in this study, indicating that an alteration of the pK_a of a catalytically important residue by D_2O is unlikely to be either masking or artificially inflating the solvent isotope effects observed here at pH 7.4. The small variation in k_{cat} with pH is consistent with the previously observed pH independence of the turnover rate under atmospheric O_2 (*37*).

Effects of Viscosogens on Steady State Parameters. In an effort to determine whether $k_{cat}/K_m(O_2)$ is limited by diffusion, the effect of increasing solution viscosity was determined using glucose, glycerol, and sucrose as viscosogens. Figure 1 shows that an increasing solution viscosity does decrease $k_{cat}/K_m(O_2)$. Other kinetic parameters in the viscosogenic buffers are summarized in Table 3. The small pH dependence of $k_{cat}/K_m(O_2)$ or k_{cat} (Table 2) indicates that a viscosogen-induced shift in the pK_a of a catalytic residue

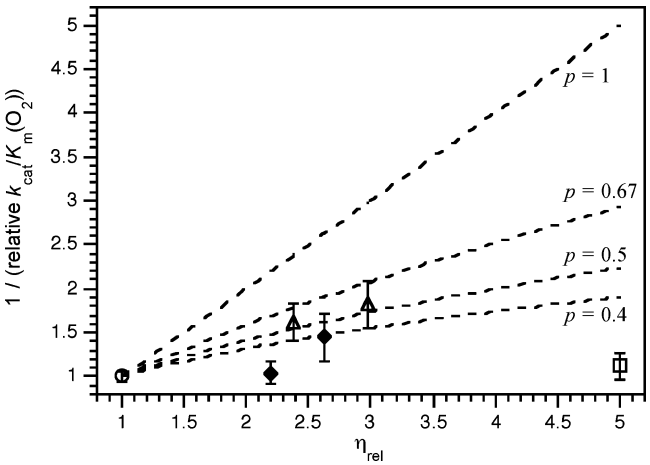

FIGURE 1: Viscosity effects on $k_{cat}/K_m(O_2)$. The relative rate and viscosity values are those from the viscosogen-containing solution divided by that from the reference solution containing no added viscosogen. Note the reciprocal nature of the *y*-axis. The dashed lines are theoretical values for a diffusion-controlled reaction given a value of *p* from eq 1. The following viscosogens were used: glucose (◆), glycerol (△), sucrose (□), and no added viscosogen (○). Rates are extrapolated to an infinite Pdx^r concentration. Conditions: 25 °C, pH 7.4, 50 mM MOPS-KOH buffer, 69 mM NaCl, and 100 μM DTT, with saturating camphor, NADH, and PdR concentrations.

Table 3: Viscosogen Effects on Steady State Kinetic Parameters[a]

viscosogen	η_{rel}	$k_{cat}/K_m(O_2)$ (μM^{-1} s^{-1})	k_{cat}/K_m(Pdx^r) (μM^{-1} s^{-1})	k_{cat} (s^{-1})	N_f[b]
none	1	0.72 (3)	27 (1)	57 (1)	1.03
23.4% glucose	2.20	0.69 (9)	11 (2)	36 (2)	0.79
31.4% glycerol	2.38	0.44 (6)	7 (1)	40 (3)	0.79
27.4% glucose	2.63	0.50 (9)	8 (2)	40 (4)	0.76
35.2% glycerol	2.98	0.40 (6)	4.4 (6)	43 (3)	0.76
37.2% sucrose	5.00	0.64 (9)	4.7 (7)	27 (2)	0.75

[a] Conditions as described in the legend of Figure 1. The O_2 concentration was varied at fixed Pdx^r concentrations, and the data were fitted to an equation for the sequential ordered mechanism as described in ref *5* to give the kinetic parameters. Errors in the last digit are in parentheses. [b] Factor used to normalize the values of k_{cat} and k_{cat}/K_m(Pdx^r) for differences in apparent O_2 solubility, obtained from the PCD/PCA assay described in Experimental Procedures. The parameter $k_{cat}/K_m(O_2)$ does not require correction because its calculation from raw initial rate data does not require the assumption of an O_2 solubility value.

(*21*, *38*) is not likely to contribute to or mask the observed viscosity effects.

Other control experiments indicate that the decrease in $k_{cat}/K_m(O_2)$ at high concentrations of glycerol and glucose may be due to a nonspecific effect on the proteins, such as a change in the dielectric constant or osmotic pressure, or inhibition by binding to the enzyme. Table 3 shows that k_{cat} is affected almost as much as $k_{cat}/K_m(O_2)$ by the viscosogens, suggesting that glycerol, glucose, and sucrose may perturb the nondiffusive steps making up k_{cat}. Though k_{cat} is thought to be limited by the first electron transfer from Pdx^r to Fe^{3+}-cam (*3*), the same inhibitory effects could show up in the O_2 binding and second electron transfer steps potentially involved in $k_{cat}/K_m(O_2)$. Observing an effect of a viscosogen on k_{cat} was somewhat surprising given a previous observation of no effect on the rate of electron transfer from Pdx^r to Fe^{3+}cam upon inclusion of 30% glucose (*39*). Table 3 and Figure 1 also show that using sucrose as a viscosogen has little effect on $k_{cat}/K_m(O_2)$. This could indicate either a

stimulatory effect of sucrose or inhibition by glucose and glycerol. Previously, an effect of glycerol was noted on the C−O stretching frequency of carbon monoxide bound at the active site iron of P450cam (*40*). This was attributed to a glycerol-induced change in the protein hydration shell. Though Figure 1 gives the appearance that $k_{cat}/K_m(O_2)$ is partially diffusion-controlled, the effects on k_{cat} and differences among the viscosogens suggest that the appearance of diffusion control may be partially or entirely an artifact of interactions of protein with the viscosogens.

One further complication of viscosity effect studies with O_2-activating enzymes (*21*, *41*) is the breakdown in the Stokes−Einstein relation for small substrates like O_2 (*42*). In more typical viscosity effect studies (*38*), the solute diffusion coefficient, and hence the rate of a diffusion-controlled reaction, is assumed to be inversely proportional to the solvent viscosity. A completely diffusion-controlled reaction would follow the line marked $p = 1$ in Figure 1 in this situation. However, for small solutes, an empirical relation between the solute diffusion coefficient (D) and solvent viscosity (η) has been found (*43*):

$$D \propto 1/\eta^p \quad (1)$$

where p is an empirical parameter with a value between 0 and 1 depending on the size of the diffusing solute relative to that of the solvent and viscosogen (*42*). For O_2, p values of 0.4 and 0.5 for diffusion through water/sucrose and water/glycerol solutions, respectively, have been calculated (*42*, *44*) from earlier electrochemical data of Jordan et al. (*45*). Other researchers have reported $p = 0.67$ in water/sucrose solutions (*46*).[2]

Of all the steady state kinetic parameters, $k_{cat}/K_m(Pdx^r)$ is the most affected by the viscosogens (Table 3). Doubling the viscosity cuts this parameter more than in half, indicating that a decrease in the affinity for Pdx^r, a decrease in k_{cat}, and the increase in solution viscosity may all contribute to the effect of viscosogen on $k_{cat}/K_m(Pdx^r)$. The affinity of Pdx for P450cam has been shown to be altered by addition of glycerol, glucose, and ethylene glycol through an osmotic pressure effect (*39*). The large viscosity effect observed here is consistent with the previous observation that k_{cat}/K_m for Pdx^r is close to its association rate constant (*5*).

Binding of O_2 to Ferrous P450cam. Previous estimates of the rate constant for binding of O_2 to ferrous P450cam (k_{on,O_2}) are 1.7×10^6 M^{-1} s^{-1}, observed in a temperature jump to 25 °C (*47*), and 0.77×10^6 M^{-1} s^{-1}, at 4 °C by stopped-flow methods (*8*). We used the same methods as the stopped-flow study (*8*) and determined a value of $(1.6 \pm 0.3) \times 10^6$ M^{-1} s^{-1} for k_{on,O_2} at 25 °C (Figure S1 in the Supporting Information). Because of the close agreement with the temperature jump measurement (*47*), no O_2 concentrations beyond the three employed in Figure S1 were used. Also, at both the highest and lowest concentrations of O_2 that were employed, the values of k_{obs} were independent of the trace Pdx and PdR concentrations used in the initial reduction of P450cam and of the fraction of ferric P450cam formed by autoxidation due to O_2 leakage prior to the measurement.

The value of 84 ± 23 s^{-1} was determined for k_{off,O_2} from the y-intercept of the k_{obs} versus O_2 concentration plot in Figure S1. This is much higher than the previous estimate of 1.1 s^{-1} at 4 °C (*8*), even considering the difference in temperature. The k_{off,O_2} at 4 °C (*8*) was determined by displacement of the O_2 ligand with carbon monoxide, which is generally regarded as a better method for determining a k_{off}. The value of k_{off,O_2} determined here is likely to be an overestimate of the true value at 25 °C, given the previous measurement at 4 °C and the observation, discussed below, of near-complete formation of oxyP450cam from Fe^{2+}cam at ~300 μM O_2 and 25 °C.

Reduction of OxyP450cam by Pdx^r. The rate of transfer of the electron from Pdx^r to oxyP450cam was previously studied at 4 °C (*3*, *10*, *11*, *48*), and the solvent isotope effect was determined at 8 °C (*17*). Here the reaction is studied at 25 °C by using a double-mixing stopped-flow method to preform the somewhat unstable oxyP450cam (*8*). The reaction between oxyP450cam and Pdx^r employs an inhibitor, metyrapone, to rapidly trap the ferric P450cam after a single turnover as described by Brewer and Peterson (*3*, *10*). The spectra of the species involved in the reaction are shown in Figure 2C. After mixing is carried out, the reaction shows the expected biphasic behavior (*3*, *10*), as indicated in Figure 2A. The 420 nm peak of Fe^{3+}mtp grows in during the first phase. After reaching a maximum level ~11 ms after mixing, excess Pdx^r reduces Fe^{3+}mtp to the ferrous, metyrapone-bound form (Fe^{2+}mtp) in the second phase.

The second phase of the reaction shows the expected spectral changes for the Fe^{3+}mtp to Fe^{2+}mtp conversion as previously noted (*10*). A decrease at 420 nm, an increase at 440 nm, and an isosbestic point at 429 nm are all observed (Figure S2), in accordance with the authentic spectra (Figure 2C). The spectral changes accompanying the first phase are more complex, showing no true isosbestic point (Figure 2B). This may be due to an encroachment of the second phase into the first (*10*) or multiple reactions contributing to the first phase. Compared to the authentic spectra in Figure 2C, the absorbance changes for the first phase (Figure 2B) do not match those expected for a simple oxyP450cam to Fe^{3+}-mtp conversion. The Soret band of the starting material appears to be shifted to wavelengths lower than those of oxyP450cam as judged by the λ_{max} of 414 nm of the first spectrum (1.9 ms after mixing) and fact that the absorbance decrease at 395 nm is almost as large as the increase at 420 nm.

A control experiment without added Pdx^r (except for the small amount used for initial P450cam reduction) showed peaks at 418−419 and 455 nm, as expected for oxyP450cam (*8*). This demonstrates that the lower-than-expected λ_{max} of the first spectrum in the reaction between Pdx^r and oxyP450cam is not due to contamination by the 391 nm-absorbing Fe^{3+}cam form. It also demonstrates that the consumption of O_2 by the scrubbing system during the aging time is not fast enough to interfere with the reaction; otherwise, a significant fraction of Fe^{2+}cam would have been observed. The oxyP450cam spectrum persisted without change for at least 450 ms in this control experiment, indicating no direct reaction between metyrapone and the oxyP450cam form as indicated previously (*3*).

[2] One further caution on using the measured diffusion coefficients as a benchmark for viscosity effects on $k_{cat}/K_m(O_2)$ should be noted. In the measurements of Jordan et al. (*45*) for data below 15% sucrose and below 20−35% glycerol, the diffusion coefficient of O_2 was greater than that predicted by the $1/\eta^p$ dependence.

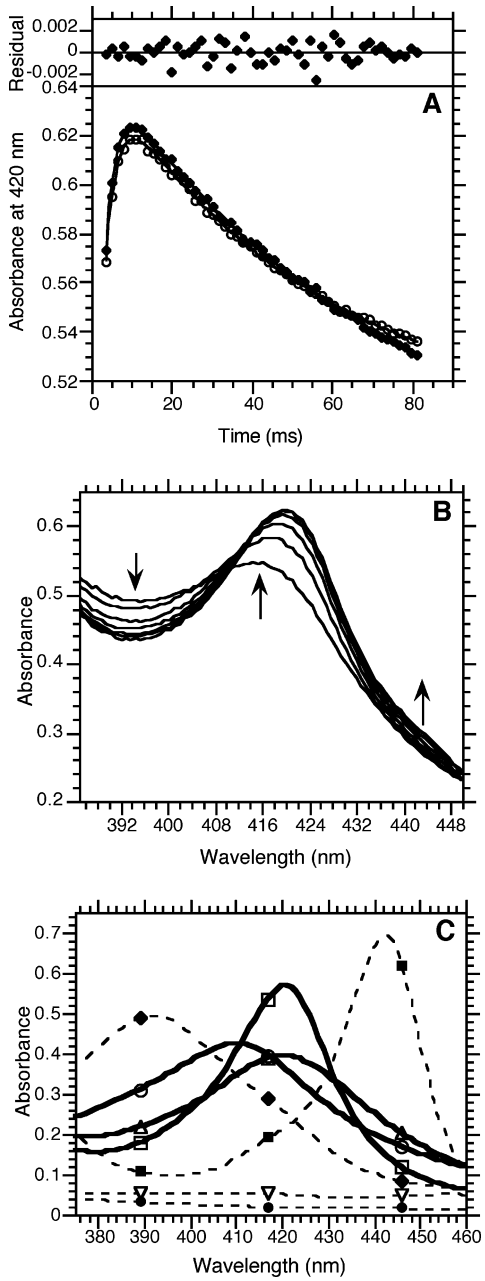

FIGURE 2: Reaction between oxyP450cam and Pdx^r. Conditions after mixing: 5 μM oxyP450cam, 25 μM camphor (total), ~300 μM O_2, 25 μM Pdx^r, 2.5 mM metyrapone, pH/pD 7.4, and 25 °C. (A) Time traces at 420 nm in buffers containing H_2O (◆) and D_2O (○) with a biexponential fit, with data from 3.4 to 85 ms after mixing. (B) Spectral changes from the first phase of the reaction in H_2O: 1.9 to 10.9 ms after mixing, all spectra; small increase in absorbance at 440 nm due to formation of Fe^{2+}met as the second phase encroaches on the first. (C) Authentic UV−visible spectra recorded (as described in Experimental Procedures) for comparison to stopped-flow data with traces in bold emphasized in the discussion. Spectra of 5 μM P450cam: Fe^{2+}cam (○), oxyP450cam (△), Fe^{3+}met (□), Fe^{2+}met (■), and Fe^{3+}cam (◆). Spectra of 5 μM Pdx: Pdx^{ox} (▽) and Pdx^r (●).

In addition to controls in the absence of added Pdx^r, several control experiments on the complete reaction were necessary. The rate of the first phase of the reaction was unaltered by doubling the camphor or metyrapone concentrations and decreased by only ~10% upon halving the O_2 concentration used to form oxyP450cam in the first stage of mixing. The first phase rate was independent of the aging time over the range of 20−100 ms (for formation of oxyP450cam) and of the Pdx^r concentration over the range of 12.5−40 μM. It did decrease when the Pdx^r concentration was reduced to 5 μM. In this reaction, the first spectrum exhibited a λ_{max} of 416 nm, which is closer to the value expected for oxyP450cam than that observed with higher concentrations of Pdx^r, demonstrating a Pdx^r concentration dependence to the observed spectral shift.

The rate of the first phase was sensitive to the conditions used to reduce the P450cam sample. Initial experiments with lower concentrations of PdR, Pdx, or glucose oxidase resulted in lower rates for the first phase of the single-turnover reaction. Invariably, there was some leakage of atmospheric O_2 into the solutions during preparation and loading into the stopped-flow apparatus. Excessively long aging times, such as 5000 ms, also resulted in reduced first-phase rates. These observations are likely all related to the same phenomenon: they would result from a greater portion of Fe^{3+}cam contaminating the oxyP450cam sample. Any Fe^{3+}cam contaminating the sample could be converted to Fe^{3+}mtp by either of two slower pathways: direct displacement of camphor by metyrapone or reduction by Pdx^r to Fe^{2+}cam followed by O_2 binding to follow the normal reaction pathway. The few data points available for the first phase may make deviations into more phases difficult to observe. For these reasons, the amounts of PdR, Pdx, and the O_2 scrubbing system employed in reduction of the P450cam solution were carefully optimized such that cutting one or two of these concentrations in half from those listed in Experimental Procedures did not result in a rate decrease greater than the experimental error.

Despite all of these caveats, the time trace at 420 nm as shown in Figure 2A fit well to a biexponential function as shown by the random residuals, yielding observed rate constants of 390 ± 23 s^{-1} for the first phase and 13.8 ± 0.8 s^{-1} for the second (average of six reactions). Fitting the data at 391 nm resulted in rate constants of 365 ± 40 and 17 ± 2 s^{-1} for the two phases. Although the spectra for the first phase do not meet in a perfect isosbestic point, the match appears to be close enough to give similar rates at several wavelengths. The data could also be fit to a single exponential at the cleaner 429 nm isosbestic point of the second phase, giving an observed rate constant of 390 ± 25 s^{-1}. Previous measurements for the rate of this reaction at 4 °C are 140 (*48*), 80 (*3*), and ~85 s^{-1} (*11*). The value of 390 s^{-1} for $k_{et,2}$ measured here at 25 °C is reasonable given these earlier measurements if the temperature dependence is similar to that observed for the first electron transfer from Pdx^r to Fe^{3+}cam ($k_{et,1}$) (*4*). Also, the closeness of k_{cat} to $k_{et,1}$ is consistent with all other first-order steps, including $k_{et,2}$, being much larger than $k_{et,1}$.

This reaction was repeated in D_2O, and the time course shows very little difference from the H_2O reaction (Figure 2A). The average of four measurements in D_2O gave observed rate constants of 361 ± 12 and 19 ± 1 s^{-1} for the first and second phases at 420 nm, respectively, yielding a solvent isotope effect of 1.08 ± 0.07 on the first phase. When compared at the other wavelengths that are noted, the D_2O effects on the first phase were similarly small and nearly within error of unity (1.20 ± 0.17 at 391 nm and 1.11 ± 0.09 at 429 nm). One difficulty in making this measurement is worth noting. Initially, a much slower rate was observed

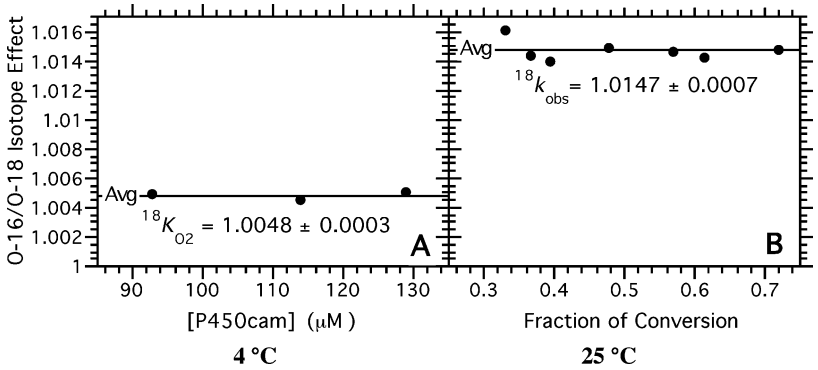

FIGURE 3: Comparison of $^{16}O/^{18}O$ equilibrium and kinetic isotope effects. (A) Equilibrium isotope effect, $^{18}K_{O_2}$, on binding of O_2 to P450cam at 4 °C in 50 mM potassium phosphate buffer (pH 7.4) and 1 mM camphor. (B) Kinetic isotope effect, $^{18}k_{obs}$, on O_2 consumption at 25 °C in 4 μM Pdx and saturating PdR with other conditions as described in the footnote of Table 4.

Table 4: Observed $^{16}O/^{18}O$ Kinetic Isotope Effects[a]

entry	reaction type[b]	[Pdx] (μM)	[P450cam] (μM)	[PdR] (μM)	$^{18}k_{obs}$	N[c]	r[d]
1	saturating PdR	4.0	0.013	0.35	1.0147 (7)	7	0.93
2	saturating PdR	1.0	0.030	1.2	1.012 (4)	6	0.92
3	saturating PdR	0.40	0.030	1.6	1.011 (2)	5	0.85
4	near-saturating PdR	0.40	0.030	0.80	1.012 (4)	4	0.87
5	background	4.0	−	0.35	1.023 (5)	5	−
6	background	0.40	−	1.6	1.019 (6)	6	−
7	limiting PdR	4.0	0.10	0.025	1.0058 (6)	3	>0.95

[a] Reactions at 25 °C. Conditions as described in the legend of Figure 1 with initial concentrations of 1 mM camphor, ~440 μM O_2, and 0.5−1 mM NADH. Standard deviations in the last digit are in parentheses. [b] Saturating PdR: [PdR] = 10*$[PdR]_{half-max}$. Near-saturating PdR: [PdR] = 5*$[PdR]_{half-max}$. Background: no P450cam. [c] Number of replicate measurements. [d] Fraction of total rate due to P450cam reaction (as opposed to background) based on initial rate measurements.

for the first phase of the reaction in D_2O. It was demonstrated, however, that this was due to incomplete reduction of P450cam or poor O_2 scrubbing. It is possible that, if the O_2 scrubbing and P450cam reduction conditions were further optimized in D_2O, the measured solvent isotope effect would be even closer to unity.

$^{16}O/^{18}O$ Equilibrium Isotope Effect. The EIE for O_2 binding ($^{18}K_{O_2}$) was measured previously for myoglobin and several other oxygen carrier proteins (*29*). Because oxyP450cam is not nearly as stable as oxymyoglobin, decomposing to the Fe^{3+}cam form with a 3 min half-life at 23 °C (*8*), the previous procedures were modified. Lowering the temperature to 4 °C increased the half-life for autoxidation of oxyP450cam to 50 min under our conditions, slightly longer than that previously reported at this temperature (*8*), and reaction of oxyP450cam with potassium ferricyanide inside the vacuum line prevented any further autoxidation during O_2 collection.

The modified methods were validated using myoglobin. An EIE of 1.0054 ± 0.0006 (N = 3, where N is the number of replicates) was previously measured for binding of O_2 to sperm whale myoglobin at room temperature (*29*). Using the methods described in this study, a value of 1.004 ± 0.002 (N = 10) was obtained for myoglobin from horse skeletal muscle at 20 °C. When the temperature was lowered to 4 °C, the EIE was 1.003 ± 0.001 (N = 5). The results with myoglobin here showed near-quantitative recovery of the bound O_2 from oxymyoglobin on the basis of a comparison of measured pressures of the blank and myoglobin samples with the known solubility of O_2 and the spectrophotometrically determined oxymyoglobin concentration (*49*).

With oxyP450cam, an EIE of 1.0048 ± 0.0003 (N = 3) was measured (Figure 3A). The extent of autoxidation at the point these samples were taken into the vacuum line was 15−21%. On the basis of this fraction and the total concentration of P450cam, 89−105% of the expected O_2 was recovered from oxyP450cam in these samples.

$^{16}O/^{18}O$ Kinetic Isotope Effect. The $^{16}O/^{18}O$ KIE on O_2 consumption at 4 μM Pdx^r was determined to be 1.0147 ± 0.0007 (N = 7) (Table 4, entry 1). This value is an estimate of the limiting KIE on $k_{cat}/K_m(O_2)$, $^{18}[k_{cat}/K_m(O_2)]$, because the apparent $k_{cat}/K_m(O_2)$ is nearly independent of the Pdx^r concentration in this range (*5*). The KIE on the background reaction at 4 μM Pdx with 0.35 μM PdR (no P450cam) was 1.023 ± 0.005 (N = 5). Because this background reaction represents only 7% of the total rate of oxygen consumption, the correction to the observed KIE (to 1.0141) is within experimental error using a simple weighted-average expression (*35*). Though the relative contributions of the background and P450cam reactions were determined from initial rates, the independence of $^{18}k_{obs}$ on the fraction of conversion (Figure 3B) demonstrates that the relative contribution of the background reaction to the total does not change significantly over the course of the reaction.

The $^{16}O/^{18}O$ KIE measurement was repeated at lower concentrations of Pdx^r (Table 4, entries 2 and 3), with the KIE decreasing to 1.011 ± 0.002 at 0.4 μM Pdx^r. Though the measurement at 0.4 μM Pdx^r shows more enzyme inactivation and has a higher background contribution than that at 4.0 μM Pdx^r due to an increased PdR requirement at lower Pdx concentrations (*5*), the KIE at 0.4 μM Pdx^r was again independent of the fraction of conversion (Figure S3). The isotope effect on the background reaction at 0.4 μM Pdx and 1.6 μM PdR was 1.019 ± 0.006 (N = 6). The observed KIE for the reaction at 0.4 μM Pdx^r in the presence of P450cam can be corrected for the background contribution to 1.010, again within experimental error of the measured

value. As a control, the KIE at 0.4 μM Pdx was repeated at a lower concentration of PdR (Table 4, entry 4) to confirm PdR saturation in the measurements at subsaturating Pdx levels.

Lowering the PdR concentration was taken to the extreme in entry 5 of Table 4. Here, the reaction rate is independent of the P450cam concentration and nearly first-order in PdR, indicating that the rate of reduction of Pdx by PdR limits the overall turnover rate (*5*). Under these conditions, the KIE on O_2 consumption was 1.0058 ± 0.0006, which is very close to the EIE measured for O_2 binding (1.0048 ± 0.0003).

DISCUSSION

Solvent Isotope Effects. The small solvent isotope effect of 1.21 ± 0.08 on $k_{cat}/K_m(O_2)$ indicates that the steps contributing to this parameter do not involve a significant degree of proton transfer,[3] in accord with studies on several other O_2-activating enzymes (*21*, *22*, *24*, *41*). The lack of a discernible solvent isotope effect on k_{cat} observed here is in agreement with the previous measurement of no D_2O effect on the first electron transfer step from Pdx^r to Fe^{3+}cam (*17*) [combined with the observation that k_{cat} is mostly limited by this first electron transfer step (*3*)] but in contrast with a previous measurement of 1.5−1.7 for the D_2O effect on the turnover rate (*19*). The turnover rate measurement was carried out under conditions similar to those employed here, except it is unclear if PdR was saturating in the previous study.

A small solvent isotope effect of 1.08 ± 0.07 to 1.20 ± 0.17 is also determined here at 25 °C for the transfer of an electron from Pdx^r to oxyP450cam. A previous measurement at 8 °C yielded a larger solvent isotope effect of 1.80 ± 0.05 on this reaction (*17*). A solvent isotope effect observed on the transfer of an electron from methylamine dehydrogenase to amicyanin was rationalized as arising from a proton transfer step that gates a subsequent long-range electron transfer step (*50*). It is possible that the proton and electron transfer steps in P450cam have different temperature dependencies, making it feasible that the apparent discrepancy between this measurement and previous measurements (*17*) is due to a temperature dependence of the solvent isotope effect. Alternatively, these findings call into question the importance of proton coupling during this long-range electron transfer step in the wild-type enzyme.

Reduction of OxyP450cam. In the reaction between Pdx^r and oxyP45cam at 25 °C, the spectral changes were somewhat different than expected for the simple electron transfer followed by subsequent rapid steps and inhibitor trapping to form Fe^{3+}mtp. This may only be a feature of the reaction at 25 °C, but others (*11*) have noted the possibility that this occurred in the earlier studies at 4 °C (*3*, *10*), where detection at only a few selected wavelengths was possible.

After incomplete reduction of the resting ferric P450cam is ruled out, there are several possible reasons that the Soret band of the starting material appears to be shifted to wavelengths lower than the 418 nm absorbance of oxy-P450cam. (1) The absorbance spectrum of oxyP450cam could be perturbed prior to electron transfer as observed by Glascock et al. (*11*). Also, in the D251N mutant of oxyP450cam, Pdx^r binding shifts the Soret band by several nanometers (*18*, *37*). (2) There could be a new intermediate in the reaction, which absorbs at a lower wavelength. In the mammalian P450 2B4 system, there is evidence of a new intermediate in the reaction between oxyP450 2B4 and a modified form of its reductase (*51*); in this instance, oxidation of the reductase occurs more rapidly than P450 returns to its resting state. In the reaction between oxyP450cam and Pdx^r at 4 °C, Brewer and Peterson carefully demonstrated that Pdx^r oxidation occurred at the same rate as Fe^{3+}mtp and hydroxylated product formation (*3*, *10*). It is possible the reaction at 25 °C could behave differently. (3) The binding of Pdx^r could induce an increase in the rate of dissociation of O_2 from oxyP450cam. A decrease in P450cam's O_2 affinity is expected upon Pdx^r binding by analogy to data on the CO-bound P450cam (see below). If the O_2 dissociation rate approached the rate of electron transfer, then a portion of the P450cam would revert to the 410 nm-absorbing Fe^{2+}cam state within the dead time of the instrument. The spectral changes for the first phase resemble the conversion of Fe^{2+}cam to Fe^{3+}mtp more than those of oxyP450cam to Fe^{3+}mtp (Figure 2). Also, in the visible region (not shown), the first spectrum at 1.9 ms after mixing with Pdx^r has a peak near 540 nm, which is near the value of both the Fe^{3+}mtp and Fe^{2+}cam and different from that of oxyP450cam (555 nm). However, we note that the observed rate was nearly independent of O_2 concentration as would be expected if the reaction proceeded largely from oxy-P450cam.

Though we hesitate to completely rule out the second and third explanations, we favor the first because a spectrally perturbed oxyP450cam intermediate (with a Soret maximum of ~414 nm) was observed in careful work by Glascock et al. during the electron transfer reaction between oxyP450cam and Pdx^r at 4 °C (*11*). Given the rapid rate of formation of this intermediate at 4 °C, it would likely be formed within the dead time of our instrument at 25 °C.

Comparison of Rate Constants. Estimates for all the rate constants potentially involved in $k_{cat}/K_m(O_2)$ have been made at 25 °C and are summarized in Table 5. It appears that the experimental value of $k_{cat}/K_m(O_2)$ is approximately half that of the measured k_{on,O_2}. Normally, this would suggest that $k_{cat}/K_m(O_2)$ is approximately half limited by O_2 binding and half

Table 5: Summary of Kinetic Parameters and Rate Constants for P450cam Measured at 25 °C, pH 7.4, and an Ionic Strength of 0.1 M

parameter	value
k_{on,O_2} (μM^{-1} s^{-1})	1.6 ± 0.3[a]
	1.7[b]
k_{off,O_2} (s^{-1})	$<84 \pm 23$[a]
$k_{et,2}$ (s^{-1})	390 ± 23[a]
$k_{et,1}$ (s^{-1})	(35−42)[c]
$k_{cat}/K_m(O_2)$ (μM^{-1} s^{-1})	0.72 ± 0.03[d]
k_{cat} (s^{-1})	55 ± 1[d]

[a] From this work. [b] From ref *47*. [c] From refs *4*, *39*, *48*, and *68*. At pH 6.7−7.4, 20−25 °C, and an ionic strength of 0.15−0.2 M. [d] From ref *5*.

[3] It is formally possible that a solvent isotope effect on $k_{cat}/K_m(O_2)$ of this size could arise from the fact that D_2O has a viscosity of ~1.2 relative to H_2O (*33*) if $k_{cat}/K_m(O_2)$ were diffusion-controlled. Earlier measurements indicated a solvent isotope effect of 1.00 ± 0.03 on the rate of binding of O_2 to Fe^{2+}cam at 20 °C (*17*), though a small increase in O_2 solubility in D_2O over that in H_2O could partially mask a solvent isotope effect on O_2 binding.

limited by the long-range electron transfer from Pdx^r, but this would require that k_{off,O_2} and $k_{et,2}$ be approximately equal according to the expression for $k_{cat}/K_m(O_2)$ derived from the mechanism in Scheme 1 as shown in eq 2:

$$k_{cat}/K_m(O_2) = \frac{k_{on,O_2}k_{et,2}}{k_{off,O_2} + k_{et,2}} \quad (2)$$

Though k_{off,O_2} is the least well defined of the parameters in Table 5, it is clear that k_{off,O_2} is much lower than $k_{et,2}$.

The most likely cause of the discrepancy among the measurements of the four parameters in eq 2 is in the assumption that k_{on,O_2} and k_{off,O_2} are unaffected by Pdx^r binding. It is known that binding of carbon monoxide to the Fe^{2+}cam form of P450cam decreases the affinity for Pdx^r markedly. For binding of Pdx^r to Fe^{2+}cam-CO, K_D values of 13 μM at 25 °C (*14*), 26 ± 12 μM at 17 °C (*16*), and 140 μM at 40 °C (*12*) have been measured. These are all much higher than the reported K_D of 0.5 μM for binding of Pdx^r to Fe^{2+}cam at 10 °C (*52*). From a thermodynamic cycle, the affinity for CO must also decrease when Pdx^r binds. It is likely that the O_2 affinity of Fe^{2+}cam would show a similar decrease upon Pdx^r binding. The EPR spectrum of Pdx^r when complexed with Fe^{2+}cam exhibited very similar shifts resulting from binding of CO, NO, and O_2 to the heme (the last one employed the D251N mutant of P450cam) (*53*).

Given the large impact of CO on Pdx^r association (*12*, *14*, *16*), Pdx^r binding may sufficiently increase k_{off,O_2} that it approaches $k_{et,2}$ in magnitude (though we expect that the value of k_{off,O_2} in Table 5 is already an overestimate). This was mentioned above as one explanation for the unexpected transient spectral changes. We cannot rule out the possibility that Pdx^r to oxyP450cam electron transfer partially contributes to $k_{cat}/K_m(O_2)$, which is explored in greater detail in the context of measured kinetic ^{18}O isotope effects. An alternative interpretation is that $k_{cat}/K_m(O_2)$ is limited largely by the O_2 binding process because $k_{off,O_2} < k_{et,2}$. The expected increase in $K_d(O_2)$ upon Pdx^r binding supports this idea because a Pdx^r binding-induced decrease in k_{on,O_2} of only 2-fold would bring the measurements of $k_{cat}/K_m(O_2)$ and k_{on,O_2} into agreement. A previous report (*54*) indicated that O_2, CO, and NO bind to Fe^{2+}cam at the same rate in both the presence and absence of Pdx^r, but given the large K_d values for binding of Pdx^r to Fe^{2+}cam-CO, it is unclear if Pdx^r was saturating in the previous study.

Viscosity Effects on $k_{cat}/K_m(O_2)$. Viscosity effects are one way to determine if diffusive steps, such as substrate binding, contribute to k_{cat}/K_m and can sometimes be used to determine quantitatively the degree of forward commitment of the substrate (the ratio of $k_{et,2}$ to k_{off,O_2} for the mechanism in Scheme 1) (*38*). They were employed here to examine whether $k_{cat}/K_m(O_2)$ is limited largely by O_2 binding. However, the viscosity effects on $k_{cat}/K_m(O_2)$ in the P450cam system are difficult to interpret. Although the use of glucose or glycerol as viscosogens could indicate that O_2 binding is at the diffusion limit (depending on which *p* value is most accurate), the fact that there are similar effects on k_{cat} argues that the observed effects are due to inhibition by the viscosogens. This is supported by the very small impact of 37.2% sucrose on $k_{cat}/K_m(O_2)$.

It is conceivable that $k_{cat}/K_m(O_2)$ could be limited by the overall oxyP450cam forming process and still show no viscosity effect, because of the multistep nature of binding of O_2 to heme proteins. The binding of O_2 and CO to myoglobin has been formulated to include ligand diffusion through the solvent to the protein, movement through the protein matrix, and reaction at heme iron (*55*−*57*). From photolysis yields, binding of O_2 to myoglobin was proposed to be limited by approximately equal contributions from the latter two steps, while CO binding was proposed to be primarily limited by reaction at the heme (*57*). This is supported by the lack of a viscosity effect on the CO binding rate at room temperature (*58*). At low temperatures, a $1/\eta^{0.5}$ dependence of both O_2 (*55*) and CO (*44*, *55*) binding rates has been explained as being due to either an effect of solution viscosity on the internal protein motions necessary for ligand movement through the protein matrix (*55*, *56*) or the expected viscosity dependence for diffusion of O_2 through glycerol/water mixtures (*44*). The fact that O_2 binds to P450cam 10 times more slowly than to myoglobin (*47*, *49*) suggests that binding of O_2 to P450cam is not likely to be limited by diffusion through solution. It is unclear whether movement through the protein or reaction at the heme limits the k_{on,O_2} in P450cam. The former might be accompanied by a viscosity effect (*55*, *56*), though the data presented here do not provide unambiguous evidence of any viscosity effect on $k_{cat}/K_m(O_2)$. The more reliable $^{16}O/^{18}O$ KIE data presented below indicate that reaction at the heme is at least partially rate-limiting.

Equilibrium Isotope Effect. The above-described measurements gave a $^{16}O/^{18}O$ EIE for binding of O_2 to P450cam of 1.0048 ± 0.0003, which can be compared to the published value of 1.0054 ± 0.0006 for sperm whale myoglobin (*29*) or the values of 1.004 ± 0.002 at 20 °C and 1.003 ± 0.001 at 4 °C for horse muscle myoglobin measured in this study. The latter indicates that the impact of changing the temperature between 4 and 25 °C will lie in the noise of the measurements. The similarity of these values may be surprising given the large difference in the electron donating ability of the two axial ligands to the heme iron (thiolate for P450cam and imidazole for myoglobin), but the O−O stretching frequencies estimated for oxymyoglobin (~1131 cm^{-1}) (*59*) and measured for oxyP450cam (1140 cm^{-1}) (*7*) indicate a very similar O−O bond order in the two complexes. Frequencies and bandwidths of the other oxygen-centered vibrational modes were also similar in these proteins (*7*).

The EIE for binding of O_2 to P450cam was measured without Pdx bound because the presence of even the oxidized form of Pdx greatly accelerates the decay of oxyP450cam (*8*). Many studies have probed the effect of Pdx complexation on the heme environment of P450cam (*12*−*16*, *18*, *53*). One resonance Raman study on the oxyP450cam form of the D251N mutant (*18*) demonstrated that Pdx^r binding resulted in a small population shift toward a conformational substate with 9 and 15 cm^{-1} lower frequencies in the O−O and Fe−O stretching bands, respectively. These shifts would be too small to measurably influence the EIE given the large change in the υ_{O-O} of 1580 cm^{-1} in molecular O_2 (*60*) to 1140 cm^{-1} in oxyP450cam (*7*).

Interpreting the $^{16}O/^{18}O$ KIE on $k_{cat}/K_m(O_2)$. An expression for the isotope effect on $k_{cat}/K_m(O_2)$ for the mechanism in Scheme 1 is (*35*)

$$^{18}[k_{cat}/K_m(O_2)] = \frac{^{18}k_{et,2}\,^{18}K_{O_2} + ^{18}k_{on,O_2}\dfrac{k_{et,2}}{k_{off,O_2}}}{1 + \dfrac{k_{et,2}}{k_{off,O_2}}} \quad (3)$$

The bulk of the evidence presented here indicates that $k_{cat}/K_m(O_2)$ is largely limited by the dioxygen binding step. In this case, eq 3 is reduced to $^{18}[k_{cat}/K_m(O_2)] \cong {}^{18}k_{on,O_2}$ (because $k_{off,O_2} \ll k_{et,2}$). The value of $^{18}k_{on,O_2}$ can be approximated as the observed KIE of 1.0147 ± 0.0007, yielding insight into the nature of the O_2 binding mechanism. The observation of a KIE on k_{on,O_2} significantly greater than unity indicates that reaction at the iron center is fully, or at least partially, rate-limiting in P450cam; movement of O_2 into and through the protein is expected to result in no change in bond order at the oxygen atoms and, hence, no isotope effect.

P450cam represents a unique case in which both the kinetic and equilibrium isotope effects on binding of O_2 to a metalloprotein have been measured. That the value of $^{18}k_{on,O_2}$ could exceed that of $^{18}K_{O_2}$ (Figure 3) is somewhat surprising as it requires a normal (>1) $^{16}O/^{18}O$ KIE in both the O_2 association and dissociation directions. Such a situation would arise if binding of O_2 to the ferrous heme within the active site follows the mechanism in Scheme 2, where a rate-limiting outer-sphere electron transfer to form ferric iron and $O_2^{\bullet-}$ is followed by a rapid collapse of the superoxide onto the iron. This type of O_2 binding mechanism was proposed to account for the very similar $^{18}[k_{cat}/K_m(O_2)]$ of 1.015 observed in methane monooxygenase (*28*). $^{16}O/^{18}O$ KIEs of 1.01−1.03 have been measured on several enzymatic reactions believed to be limited by outer-sphere electron transfers to O_2 that form the superoxide anion, accompanied by varying degrees of transition state interaction with an active site metal (*20*−*25*, *27*). In light of the multiple pathways with varying spin state changes that have been described for the addition of O_2 to heme iron proteins (cf. ref *61*), we would expect our measured KIE for P450cam to reflect average changes in bond order to O_2 for the aggregate of such pathways.

An alternative mechanism for binding of O_2 to the heme iron could involve an inner-sphere electron transfer, such as the encounter complex mechanism described for binding of O_2 to a Co^{2+} porphyrin model compound (*62*). However, this appears to be incompatible with the observation that the KIE for O_2 binding exceeds the EIE in P450cam by a large margin; formation of an encounter complex between O_2 and ferrous iron would have a very small isotope effect due to little rearrangement in bonding at the oxygen atoms, and the KIE on the second step of electronic rearrangement to form the ferrous superoxide complex should not greatly exceed the measured EIE for O_2 binding (provided that the transition state for electronic rearrangement is not largely asymmetric). Though an asynchronous reaction, where the π bond of O_2 breaks before the Fe−O bond forms, may result in a KIE that is larger than the EIE for the step, this scenario begins to become indistinguishable from the outer-sphere electron transfer mechanism for O_2 binding. One property that could increase the magnitude of the KIE for an inner-sphere complex reaction is the presence of an isotopically sensitive reaction coordinate frequency that enters into the kinetic isotope effect expressions when electron transfer is accompanied by bond formation. However, estimates from a study of Roth and co-workers indicate that this is likely to be too small [≤ 1.007 (*63*)] to significantly inflate the measured KIE for P450cam to its experimental value.

Scheme 2: Outer-Sphere Electron Transfer Mechanism for Binding of O_2 to Ferrous Heme within the Active Site of P450cam

$$Fe^{2+}\ \ O_2 \rightleftharpoons Fe^{3+}\ \ O_2^{\cdot-} \rightleftharpoons Fe^{3+}\text{–}O_2^{\cdot-}$$

A second feature that could elevate the measured KIE on $k_{cat}/K_m(O_2)$ above the EIE for O_2 binding is the contribution of another isotopically sensitive step after formation of oxyP450cam. Though the evidence presented above strongly favors a mechanism in which $k_{cat}/K_m(O_2)$ is almost fully limited by O_2 reaction at the heme iron, it is not possible to exclude the possibility that the long-range electron transfer from Pdx^r to the oxy P450cam contributes somewhat to $k_{cat}/K_m(O_2)$. In the situation where k_{off,O_2} approximates $k_{et,2}$, eq 3 shows that the term $^{18}K_{O_2}\,^{18}k_{et,2}$ deriving from the long-range electron transfer step contributes to $^{18}[k_{cat}/K_m(O_2)]$ along with the term $^{18}k_{O_2}$ from the O_2 binding step. If this long-range electron transfer is not controlled by conformational gating (*64*), a significant $^{16}O/^{18}O$ KIE is expected as a peroxo species forms from oxyP450cam (Scheme 1). The $k_{et,2}$ step in the D251N mutant of P450cam is slowed greatly in comparison to that of the wild-type enzyme (*18*). Further studies of the $^{16}O/^{18}O$ KIE in this mutant of P450cam would be of interest and may provide boundary conditions for the extent to which an interprotein electron transfer could contribute to the isotopic discrimination in the reaction of the wild-type enzyme.

Kinetic Order of Pdx^r and O_2 Binding. For the steps leading up to the second electron transfer event, we previously proposed a kinetic mechanism shown in Scheme 1 in which Fe^{2+}cam binds Pdx^r before O_2 as the dominant pathway (*5*). This proposal was based in part on the observation that $k_{cat}/K_m(Pdx^r)$ was very near the rate constant for Pdx^r binding along with the inability of saturating Pdx^r concentrations to force $k_{cat}/K_m(O_2)$ to approach its maximum limit of k_{on,O_2}. While the high-viscosity effects on $k_{cat}/K_m(Pdx^r)$ shown here are consistent with this parameter being limited by Pdx^r binding, measuring the isotope effect on $k_{cat}/K_m(O_2)$ as a function of Pdx^r concentration offers an alternative test of mechanism (cf. ref *65*). For an obligatory ordered mechanism with Pdx^r binding first, the isotope effect on the apparent $k_{cat}/K_m(O_2)$ should be independent of the Pdx^r concentration, while in a mechanism with either Pdx^r binding after O_2 or a random binding order, the $^{16}O/^{18}O$ KIE would vary with the Pdx^r concentration. The KIE does decrease slightly when the Pdx^r concentration is lowered from 4.0 to 0.4 μM (Table 4). Entry 7 in Table 4, where PdR limits the overall rate of turnover, can be interpreted as a case of a very low Pdx^r concentration since most of the Pdx will be in the oxidized form in steady state turnover with limiting PdR (*5*). This entry shows a significant KIE decrease compared with entries 1−3 where PdR is saturating. The value of the KIE on the overall reaction does approach the EIE for the O_2 binding step ($^{18}K_{O_2}$) in this very low Pdx^r limit. This may arise if an equilibrium between free and heme-bound O_2 is established while the next step required to commit the bound oxygen to products is very slow,

irreversible, and not isotopically sensitive. The Pdx^r binding step could fit this description when the Pdx^r concentration is very low, implying that O_2 can bind first in this extreme case and suggesting a possible random component to binding during the second electron transfer portion of the P450cam kinetic mechanism.

Others have examined the random mechanism with another enzyme exhibiting isotope effects on both substrate binding and chemistry (*66*). From this reference, we can conclude that, in the limit of saturating Pdx^r, the random mechanism will give the same expression for $^{18}[k_{cat}/K_m(O_2)]$ as shown in eq 3. This indicates that our interpretation of the $^{18}[k_{cat}/K_m(O_2)]$ at saturating Pdx^r in terms of eq 3 and Scheme 1 is valid even if there is a random component to the binding order.

Comparison with Other Dioxygen-Activating Enzymes. When saturated with its redox partners, P450cam appears similar to most other O_2-utilizing enzymes studied to date, including glucose oxidase (*21*−*23*), amine oxidase (*24*−*26*), tyrosine hydroxylase (*27*), and methane monooxygenase (*28*), in that reduction of O_2 by one electron contributes to the rate-limiting step in O_2 activation. It has been postulated that this serves to minimize accumulation of reactive oxygen species during catalysis (*20*). While P450cam's one-electron-reduced intermediate (oxyP450cam) is stable enough to be isolated and studied in contrast to the other enzymes mentioned above, during catalytic turnover (in the presence of high levels of Pdx^r) the second electron in P450cam O_2 activation appears to be fast enough to prevent accumulation of oxyP450cam. This occurs despite the fact that the second electron in P450cam O_2 activation must come from an interprotein electron transfer, in comparison to the above-mentioned proteins in which the second electron donor resides in a position proximal to the partially reduced O_2 intermediate.

The modest stability of oxyP450cam may be more important in avoiding $O_2^{\bullet-}$ release during turnover with subsaturating redox partners. In fact, accumulation of the oxyP450cam form was noted during steady state turnover with small amounts of PdR (*47*). This may also be the case in vivo, where the P450cam:Pdx:PdR ratio has been reported to be 8:8:1 (*67*). However, one should be cautious in interpreting these ratios as an indication that P450cam is subsaturated with its redox partners during in vivo turnover. The amount of PdR required to saturate the system was shown to decrease with O_2 concentration (*5*) and would likely decrease with substrate concentration. The amount of O_2 available to P450cam in the bacteria may be smaller than in the air-saturated water used in most in vitro studies.

Conclusions. Investigation of the properties of the second-order rate constant for the interaction of P450cam with O_2 indicates that the binding rate constant for O_2 is largely rate-determining. This $k_{cat}/K_m(O_2)$ is comprised of multiple steps, any of which could, in principle, dominate the rate: diffusion of O_2 to the protein, movement of O_2 through the protein to the heme iron site, transfer of an electron to the O_2 in the course of oxyP450cam formation, and, finally, the irreversible reduction of oxyP450cam to a P450−peroxy complex. From the comparison of stopped-flow to steady state kinetic parameters, and the measurement of viscosogen effects and $^{16}O/^{18}O$ binding and kinetic effects, it is concluded that the step involving transfer of a prebound O_2 to the heme iron site controls $k_{cat}/K_m(O_2)$. We cannot eliminate the possibility of some additional rate limitation by the interprotein electron transfer from Pdx^r to oxyP450cam. The small solvent isotope effects observed at 25 °C on $k_{cat}/K_m(O_2)$, k_{cat}, and Pdx^r to oxyP450cam electron transfer indicate little involvement of proton transfer in the transition states limiting each of these processes. The results with P450cam are similar to those seen with other O_2 activation enzymes (*20*), in which the first electron transfer to O_2 has been concluded to limit the early O_2 chemical events.

SUPPORTING INFORMATION AVAILABLE

A plot of k_{obs} versus O_2 concentration for binding of O_2 to P450cam (Figure S1), spectral changes accompanying the second phase of the reaction between oxyP450cam and Pdx^r (Figure S2), and a plot of $^{18}k_{obs}$ versus the fraction of conversion from measurement of the $^{16}O/^{18}O$ KIE at 0.4 μM Pdx^r (Figure S3). This material is available free of charge via the Internet at http://pubs.acs.org.

REFERENCES

1. Makris, T. M., Denisov, I. G., Schlichting, I., and Sligar, S. G. (2005) Activation of molecular oxygen by cytochrome P450, in *Cytochrome P450: Structure, Mechanism, and Biochemistry* (Ortiz de Montellano, P. R., Ed.) 3rd ed., pp 149−182, Kluwer Academic, New York.
2. Paine, M. J. I., Scrutton, N. S., Munro, A. W., Gutierrez, A., Roberts, G. C. K., and Wolf, C. R. (2005) Electron transfer partners of cytochrome P450, in *Cytochrome P450: Structure, Mechanism, and Biochemistry* (Ortiz de Montellano, P. R., Ed.) 3rd ed., pp 115−148, Kluwer Academic, New York.
3. Brewer, C. B., and Peterson, J. A. (1988) Single turnover kinetics of the reaction between oxycytochrome P-450cam and reduced putidaredoxin, *J. Biol. Chem. 263*, 791−798.
4. Hintz, M. J., and Peterson, J. A. (1981) The kinetics of reduction of cytochrome P-450cam by reduced putidaredoxin, *J. Biol. Chem. 256*, 6721−6728.
5. Purdy, M. M., Koo, L. S., Ortiz de Montellano, P. R., and Klinman, J. P. (2004) Steady-state kinetic investigation of cytochrome P450cam: Interaction with redox partners and reaction with molecular oxygen, *Biochemistry 43*, 271−281.
6. Schlichting, I., Berendzen, J., Chu, K., Stock, A. M., Maves, S. A., Benson, D. E., Sweet, R. M., Ringe, D., Petsko, G. A., and Sligar, S. G. (2000) The catalytic pathway of cytochrome P450cam at atomic resolution, *Science 287*, 1615−1622.
7. Macdonald, I. D. G., Sligar, S. G., Christian, J. F., Unno, M., and Champion, P. M. (1999) Identification of the Fe-O-O bending mode in oxycytochrome P450cam by resonance Raman spectroscopy, *J. Am. Chem. Soc. 121*, 376−380.
8. Peterson, J. A., Ishimura, Y., and Griffin, B. W. (1972) *Pseudomonas putida* cytochrome P-450: Characterization of an oxygenated form of the hemoprotein, *Arch. Biochem. Biophys. 149*, 197−208.
9. Davydov, R., Makris, T. M., Kofman, V., Werst, D. E., Sligar, S. G., and Hoffman, B. M. (2001) Hydroxylation of camphor by reduced oxy-cytochrome P450cam: Mechanistic implications of EPR and ENDOR studies of catalytic intermediates in native and mutant enzymes, *J. Am. Chem. Soc. 123*, 1403−1415.
10. Brewer, C. B., and Peterson, J. A. (1986) Single turnover studies with oxy-cytochrome P-450cam, *Arch. Biochem. Biophys. 249*, 515−521.
11. Glascock, M. C., Ballou, D. P., and Dawson, J. H. (2005) Direct observation of a novel perturbed oxyferrous catalytic intermediate during reduced putidaredoxin-initiated turnover of cytochrome P-450-CAM: Probing the effector role of putidaredoxin in catalysis, *J. Biol. Chem. 280*, 42134−42141.
12. Tosha, T., Yoshikawa, S., Takahashi, S., Ishimori, K., Shimada, H., and Morishima, I. (2003) NMR study on the structural changes of cytochrome P450cam upon the complex formation with putidaredoxin, *J. Biol. Chem. 278*, 39809−39821.
13. Unno, M., Christian, J. F., Sjodin, T., Benson, D. E., Macdonald, I. D. G., Sligar, S. G., and Champion, P. M. (2002) Complex

formation of cytochrome P450cam with putidaredoxin: Evidence for protein-specific interactions involving the proximal thiolate ligand, *J. Biol. Chem. 277*, 2547−2553.
14. Nagano, S., Shimada, H., Tarumi, A., Hishiki, T., Kimata-Ariga, Y., Egawa, T., Suematsu, M., Park, S. Y., Adachi, S., Shiro, Y., and Ishimura, Y. (2003) Infrared spectroscopic and mutational studies on putidaredoxin-induced conformational changes in ferrous CO-P450cam, *Biochemistry 42*, 14507−14514.
15. Shimada, H., Nagano, S., Hori, H., and Ishimura, Y. (2001) Putidaredoxin-cytochrome P450cam interaction, *J. Inorg. Biochem. 83*, 255−260.
16. Pochapsky, S. S., Pochapsky, T. C., and Wei, J. W. (2003) A model for effector activity in a highly specific biological electron transfer complex: The cytochrome P450cam-putidaredoxin couple, *Biochemistry 42*, 5649−5656.
17. Aikens, J., and Sligar, S. G. (1994) Kinetic solvent isotope effects during oxygen activation by cytochrome P-450cam, *J. Am. Chem. Soc. 116*, 1143−1144.
18. Sjodin, T., Christian, J. F., Macdonald, I. D. G., Davydov, R., Unno, M., Sligar, S. G., Hoffman, B. M., and Champion, P. M. (2001) Resonance Raman and EPR investigations of the D251N oxycytochrome P450cam/putidaredoxin complex, *Biochemistry 40*, 6852−6859.
19. Vidakovic, M., Sligar, S. G., Li, H., and Poulos, T. L. (1998) Understanding the role of the essential Asp251 in cytochrome P450cam using site-directed mutagenesis, crystallography, and kinetic solvent isotope effect, *Biochemistry 37*, 9211−9219.
20. Klinman, J. P. (2001) Life as aerobes: Are there simple rules for activation of dioxygen by enzymes? *J. Biol. Inorg. Chem. 6*, 1−13.
21. Roth, J. P., and Klinman, J. P. (2003) Catalysis of electron transfer during activation of O_2 by the flavoprotein glucose oxidase, *Proc. Natl. Acad. Sci. U.S.A. 100*, 62−67.
22. Su, Q. J., and Klinman, J. P. (1999) Nature of oxygen activation in glucose oxidase from *Aspergillus niger*: The importance of electrostatic stabilization in superoxide formation, *Biochemistry 38*, 8572−8581.
23. Roth, J. P., Wincek, R., Nodet, G., Edmonson, D. E., McIntire, W. S., and Klinman, J. P. (2004) Oxygen isotope effects on electron transfer to O_2 probed using chemically modified flavins bound to glucose oxidase, *J. Am. Chem. Soc. 126*, 15120−15131.
24. Su, Q. J., and Klinman, J. P. (1998) Probing the mechanism of proton coupled electron transfer to dioxygen: The oxidative half-reaction of bovine serum amine oxidase, *Biochemistry 37*, 12513−12525.
25. Mills, S. A., Goto, Y., Su, Q. J., Plastino, J., and Klinman, J. P. (2002) Mechanistic comparison of the cobalt-substituted and wild-type copper amine oxidase from *Hansenula polymorpha*, *Biochemistry 41*, 10577−10584.
26. Goto, Y., and Klinman, J. P. (2002) Binding of dioxygen to non-metal sites in proteins: Exploration of the importance of binding site size versus hydrophobicity in the copper amine oxidase from *Hansenula polymorpha*, *Biochemistry 41*, 13637−13643.
27. Francisco, W. A., Tian, G. C., Fitzpatrick, P. F., and Klinman, J. P. (1998) Oxygen-18 kinetic isotope effect studies of the tyrosine hydroxylase reaction: Evidence of rate limiting oxygen activation, *J. Am. Chem. Soc. 120*, 4057−4062.
28. Stahl, S. S., Francisco, W. A., Merkx, M., Klinman, J. P., and Lippard, S. J. (2001) Oxygen kinetic isotope effects in soluble methane monooxygenase, *J. Biol. Chem. 276*, 4549−4553.
29. Tian, G. C., and Klinman, J. P. (1993) Discrimination between O-16 and O-18 in oxygen binding to the reversible oxygen carriers hemoglobin, myoglobin, hemerythrin, and hemocyanin: A new probe for oxygen binding and reductive activation by proteins, *J. Am. Chem. Soc. 115*, 8891−8897.
30. Auclair, K., Moënne-Loccoz, P., and Ortiz de Montellano, P. R. (2001) Roles of the proximal heme thiolate ligand in cytochrome P450cam, *J. Am. Chem. Soc. 123*, 4877−4885.
31. Blackow, S. C., Raines, R. T., Lim, W. A., Zamore, P. D., and Knowles, J. R. (1988) Triosephosphate isomerase is diffusion controlled, *Biochemistry 27*, 1158−1167.
32. Whittaker, J. W., Orville, A. M., and Lipscomb, J. D. (1990) Protocatechuate 3,4-dioxygenase from *Brevibacterium fuscum*, *Methods Enzymol. 188*, 82−88.
33. Schowen, B. K., and Schowen, R. L. (1982) Solvent isotope effects on enzyme systems, *Methods Enzymol. 87*, 551−606.
34. Tonomura, B., Nakatani, H., Ohnishi, M., Yamaguchi-Ito, J., and Hiromi, K. (1978) Reduction of 2,6-dichlorophenolindophenol and potassium ferricyanide by L-ascorbic acid, *Anal. Biochem. 84*, 370−383.
35. Purdy, M. M. (2003) Ph.D. Thesis, University of California, Berkeley, CA.
36. Tian, G. C., Berry, J. A., and Klinman, J. P. (1994) O-18 kinetic isotope effects in the dopamine β-monooxygenase reaction: Evidence for a new chemical mechanism in nonheme metallomonooxygenases, *Biochemistry 33*, 226−234.
37. Gerber, N. C., and Sligar, S. G. (1994) A role for Asp-251 in cytochrome P-450cam oxygen activation, *J. Biol. Chem. 269*, 4260−4266.
38. Brouwer, A. C., and Kirsch, J. F. (1982) Investigation of diffusion-limited rates of chymotrypsin reactions by viscosity variation, *Biochemistry 21*, 1302−1307.
39. Furukawa, Y., and Morishima, I. (2001) The role of water molecules in the association of cytochrome P450cam with putidaredoxin: An osmotic pressure study, *J. Biol. Chem. 276*, 12983−12990.
40. Schulze, H., Ristau, O., and Jung, C. (1994) The carbon monoxide stretching modes in camphor-bound cytochrome P-450cam: The effect of solvent conditions, temperature, and pressure, *Eur. J. Biochem. 224*, 1047−1055.
41. Knapp, M. J., and Klinman, J. P. (2003) Kinetic studies of oxygen reactivity in soybean lipoxygenase-1, *Biochemistry 42*, 11466−11475.
42. Dunford, H. B., and Hasinoff, B. B. (1986) On the rates of enzymatic, protein and model compound reactions: The importance of diffusion control, *J. Inorg. Biochem. 28*, 263−269.
43. Hayduk, W., and Cheng, S. C. (1971) Review of the relation between diffusivity and solvent viscosity in dilute liquid solutions, *Chem. Eng. Sci. 26*, 635−646.
44. Hasinoff, B. B., and Chishti, S. B. (1982) Viscosity dependence of the kinetics of the diffusion-controlled reaction of carbon monoxide and myoglobin, *Biochemistry 21*, 4275−4278.
45. Jordan, J., Ackerman, E., and Berger, R. L. (1956) Polarographic diffusion coefficients of oxygen defined by activity gradients in viscous media, *J. Am. Chem. Soc. 78*, 2979−2983.
46. Hikita, H., Asai, S., and Azuma, Y. (1978) Solubility and diffusivity of oxygen in aqueous sucrose solutions, *Can. J. Chem. Eng. 56*, 371−374.
47. Tyson, C. A., Lipscomb, J. D., and Gunsalus, I. C. (1972) The role of putidaredoxin and P450 cam in methylene hydroxylation, *J. Biol. Chem. 247*, 5777−5784.
48. Tosha, T., Yoshioka, S., Hori, H., Takahashi, S., Ishimori, K., and Morishima, I. (2002) Molecular mechanism of the electron transfer reaction in cytochrome P450cam-putidaredoxin: Roles of glutamine 360 at the heme proximal site, *Biochemistry 41*, 13883−13893.
49. Antonini, E., and Brunori, M. (1971) *Hemoglobin and Myoglobin and Their Reactions with Ligands*, North-Holland Publishing, Amsterdam.
50. Bishop, G. R., and Davidson, V. L. (1995) Intermolecular electron transfer from substrate-reduced methylamine dehydrogenase to amicyanin is linked to proton transfer, *Biochemistry 34*, 12082−12086.
51. Zhang, H., Gruenke, L., Arscott, D., Harris, D. L., Glavanovich, M., Johnson, R., and Waskell, L. (2003) Determination of the rate of reduction of oxyferrous cytochrome P450 2B4 by 5-deazaFAD T491V cytochrome P450 reductase, *Biochemistry 42*, 11594−11603.
52. Sligar, S. G., and Gunsalus, I. C. (1976) A thermodynamic model of regulation: Modulation of redox equilibria in camphor monoxygenase, *Proc. Natl. Acad. Sci. U.S.A. 73*, 1078−1082.
53. Shimada, H., Nagano, S., Ariga, Y., Unno, M., Egawa, T., Hishiki, T., Ishimura, Y., Masuya, F., Obata, T., and Hori, H. (1999) Putidaredoxin-cytochrome P450cam interaction: Spin state of the heme iron modulates putidaredoxin structure, *J. Biol. Chem. 274*, 9363−9369.
54. Pederson, T. C., Austin, R. H., and Gunsalus, I. C. (1977) Redox and ligand dynamics in P450cam-putidaredoxin complexes, in *Microsomes and Drug Oxidations: Proceedings of the Third International Symposium* (Ullrich, V., Roots, I., Hildebrandt, A., Estabrook, R. W., and Conney, A. H., Eds.) pp 275−283, Pergamon Press, New York.
55. Beece, D., Eisenstein, L., Frauenfelder, H., Good, D., Marden, M. C., Reinisch, L., Reynolds, A. H., Sorensen, L. B., and Yue, K. T. (1980) Solvent viscosity and protein dynamics, *Biochemistry 19*, 5147−5157.
56. Steinbach, P. J., Ansari, A., Berendzen, J., Braunstein, D., Chu, K., Cowen, B. R., Ehrenstein, D., Frauenfelder, H., Johnson, J. B., Lamb, D. C., Luck, S., Mourant, J. R., Nienhaus, G. U., Ormos,

P., Philipp, R., Xie, A., and Young, R. D. (1991) Ligand binding to heme proteins: Connection between dynamics and function, *Biochemistry 30*, 3988−4001.
57. Olson, J. S., and Phillips, G. N. J. (1996) Kinetic pathways and barriers for ligand binding to myoglobin, *J. Biol. Chem. 271*, 17593−17596.
58. McKinnie, R. E., and Olson, J. S. (1981) Effects of solvent composition and viscosity on the rates of CO binding to heme proteins, *J. Biol. Chem. 256*, 8928−8932.
59. Miller, L. M., and Chance, M. R. (1995) Structural and electronic factors that influence oxygen affinities: A spectroscopic comparison of ferrous and cobaltous oxymyoglobin, *Biochemistry 34*, 10170−10179.
60. Chase, M. W., Jr., Curnutt, J. L., Downey, J. R., McDonald, R. A., Syverud, A. N., and Valenzuela, E. A. (1982) JANF thermochemical tables, 1982 supplement, *J. Phys. Chem. Ref. Data 11*, 695−940.
61. Jensen, K. P., and Ryde, U. (2004) How O_2 binds to heme, *J. Biol. Chem. 279*, 14561−14569.
62. Zou, S., Baskin, J. S., and Zewail, A. H. (2002) Molecular recognition of oxygen by protein mimics: Dynamics on the femtosecond to microsecond time scale, *Proc. Natl. Acad. Sci. U.S.A. 99*, 9625−9630.
63. Lanci, M. P., Brinkley, D. W., Stone, K. L., Smirnov, V. V., and Roth, J. P. (2005) Structures of transition states in metal-mediated O_2-activation reactions, *Angew. Chem., Int. Ed. 44*, 7272−7266.
64. Davidson, V. L. (2000) What controls the rates of interprotein electron-transfer reactions, *Acc. Chem. Res. 33*, 87−93.
65. Miller, S. M., and Klinman, J. P. (1982) Deduction of kinetic mechanisms from primary hydrogen isotope effects: Dopamine β-monooxygenase, a case history, *Methods Enzymol. 87*, 711−732.
66. Gawlita, E., Caldwell, W. S., Oleary, M. H., Paneth, P., and Anderson, V. E. (1995) Kinetic isotope effects on substrate association: Reactions of phosphoenolpyruvate with phosphoenolpyruvate carboxylase and pyruvate kinase, *Biochemistry 34*, 2577−2583.
67. Roome, P. W., Jr., Philley, J. C., and Peterson, J. A. (1983) Purification and properties of putidaredoxin reductase, *J. Biol. Chem. 258*, 2593−2598.
68. Unno, M., Shimada, H., Toba, Y., Makino, R., and Ishimura, Y. (1996) Role of Arg112 of cytochrome p450cam in the electron transfer from reduced putidaredoxin: Analyses with site-directed mutants, *J. Biol. Chem. 271*, 17869−17874.

BI061726W